

## Existence of an ultraflat band in the charge density wave state of $4H_b$ -TaS<sub>1.3</sub>Se<sub>0.7</sub>

Qingxin Liu,<sup>1,\*</sup> Peihan Sun<sup>1,\*</sup> Fanyu Meng<sup>1,\*</sup> Yanyan Geng,<sup>1,\*</sup> Zhonghao Liu,<sup>2,3</sup> Jianfeng Zhang<sup>4</sup>, Jingjing Gao,<sup>5</sup> Zhicheng Jiang,<sup>2</sup> Shangjie Tian<sup>1</sup>, Xuan Luo,<sup>5</sup> Yuping Sun,<sup>5,6,7</sup> Zhihai Cheng,<sup>1,†</sup> Kai Liu<sup>1,‡</sup>, Hechang Lei,<sup>1,§</sup> and Shancai Wang<sup>1,||</sup>

<sup>1</sup>Department of Physics, Key Laboratory of Quantum State Construction and Manipulation, Ministry of Education, Renmin University of China, Beijing 100872, China

<sup>2</sup>State Key Laboratory of Functional Materials for Informatics, Shanghai Institute of Microsystem and Information Technology, Chinese Academy of Science, Shanghai 200050, China


<sup>3</sup>Center of Materials Science and Optoelectronics Engineering, University of Chinese Academy of Sciences, Beijing 100049, China

<sup>4</sup>Institute of Physics, Chinese Academy of Sciences, Beijing 100190, China

<sup>5</sup>Key Laboratory of Materials Physics, Institute of Solid State Physics, HFIPS, Chinese Academy of Sciences, Hefei 230031, China

<sup>6</sup>High Magnetic Laboratory, HFIPS, Chinese Academy of Sciences, Hefei 230031, China

<sup>7</sup>Collaborative Innovation Centre of Advanced Microstructures, Nanjing University, Nanjing 210093, China

 (Received 26 May 2023; revised 27 July 2023; accepted 21 August 2023; published 8 September 2023)

A flat band is an electronic state with quenched kinetic energy and an extremely high density of states. In such a state, a small electron-electron correlation can drive multiple intriguing quantum phenomena. By using angle-resolved photoemission spectroscopy, we report the existence of a dispersionless flat band with a sharp quasiparticle peak below  $E_F$  in the charge density wave state of  $4H_b$ -TaS<sub>1.3</sub>Se<sub>0.7</sub>. This band extends over the  $\sqrt{13} \times \sqrt{13}$  reconstructed Brillouin zone. In combination with the density functional theory calculation, we identify that the flat band is due to the formation of the Star of David at the top-most  $T$  layer. In addition, the scanning tunneling spectroscopy observes a sharp peak above  $E_F$ . We attribute it to the electron-correlation-driven splitting, forming a small gap of  $\sim 45$  meV. Our observation of the flat band and splitting in  $4H_b$ -TaS<sub>1.3</sub>Se<sub>0.7</sub> provides a platform to manipulate the electron-correlation-related quantum phenomena at a low energy scale.

DOI: [10.1103/PhysRevB.108.115115](https://doi.org/10.1103/PhysRevB.108.115115)

### I. INTRODUCTION

The flat band with localized states and macroscopic degeneracies has recently received increasing attention due to its exotic properties and related intriguing physical phenomena. Theoretically, the flat band exhibits no dispersion, resulting in charge carriers with quenched kinetic energy and infinite effective mass. It is considered an ideal platform for exploring strongly correlated electronic states and many-body interactions. Recently, the flat band was predicted in a few frameworks, such as electronic material systems [1–3], optical lattices [4], exciton-polariton condensates [5,6], and bosonic system photonic lattices [7]. Among the electronic systems, narrow bands have been reported in CoSn and FeSn of kagome lattice [8,9], twisted bilayer graphene and twisted transition metal dichalcogenides (TMDs) in moiré super lattice systems [10–13], and in some TMDs with charge-density-wave (CDW) transition [14,15]. However, these bands are often with nonnegligible bandwidth. Searching for an ideal flat-band material is essential for studying exotic many-body quantum phases and remains a challenge.

In TMD materials with  $1T$  structure, a flat band is predicted at low temperature in the CDW state with formation of the Star of David (SD) supercell [16–18], and a Mott insulating phase has been expected for a long time [19–21]. In the bulk  $1T$ -TaS<sub>2</sub>, scanning tunneling spectroscopy (STM) has shown evidence of a Mott localized gap at low temperature [22]. However, a recent angle-resolved photoemission spectroscopy (ARPES) measurement found that interlayer coupling causes dimerization along the  $c$  axis, which destroys the Mott insulating phase and drives the system into a band insulator. Meanwhile, the dimerization also distorts the in-plane dispersion, and the flat band gains finite bandwidth [23].

Recently, investigations on monolayer  $1T$ -TaS<sub>2</sub> or heterostructures are of great interest due to their reduced dimensionality or interlayer coupling strength. The STM measurement showed a band gap in monolayer  $1T$ -TaS<sub>2</sub>, and it was attributed to a Mott insulating gap [24]. However, up to now, the confirmation of a well-defined flat band in  $\mathbf{k}$  space remains elusive, partially because the bulk  $1T$  structure has poor conductance in the CDW state. To realize a well-defined flat band and the Mott insulating phase, we did the ARPES measurement on  $4H_b$ -TaS<sub>2-x</sub>Se<sub>x</sub> with intercalated insulating  $1T$ -TaS<sub>2-x</sub>Se<sub>x</sub> and metallic  $1H$ -TaS<sub>2-x</sub>Se<sub>x</sub> layers. The intercalation of  $1H$  reduces the coupling strength along  $c$  axis and provides a conducting pathway within the material, which makes  $4H_b$ -TaS<sub>2-x</sub>Se<sub>x</sub> an ideal platform to investigate the correlation effects in the  $1T$ -TMD-related system.

\*These authors contributed equally to this work.

†zhihaicheng@ruc.edu.cn

‡kliu@ruc.edu.cn

§hleil@ruc.edu.cn

||scw@ruc.edu.cn

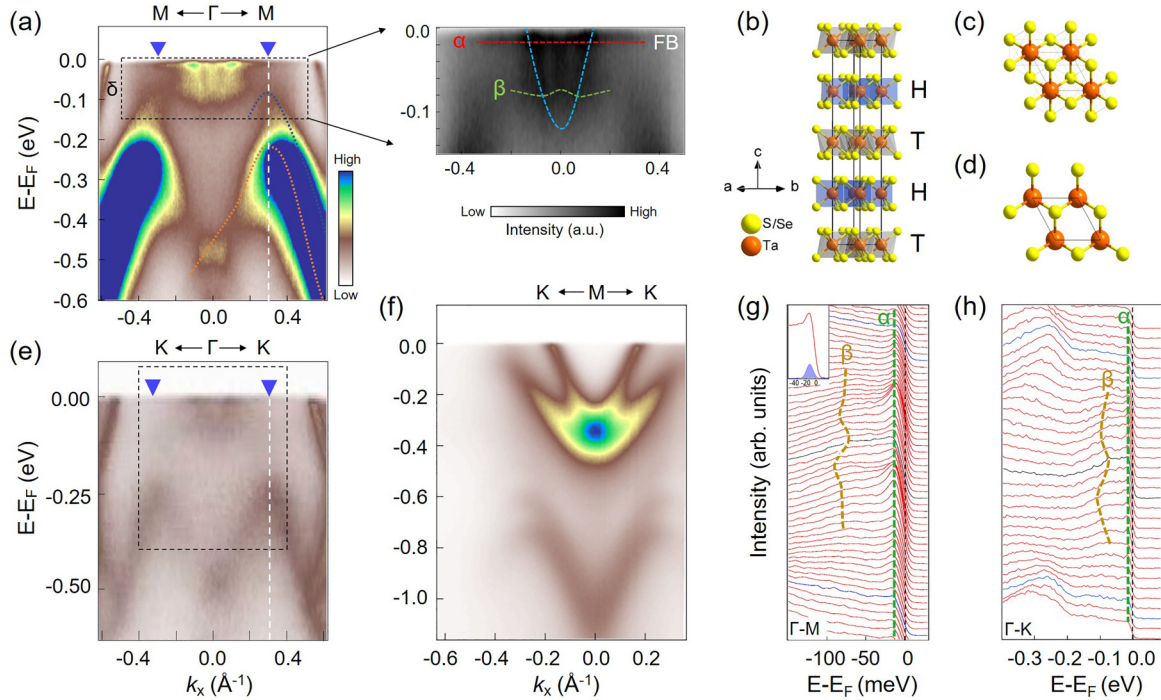


FIG. 1. Angle-resolved photoemission spectroscopy (ARPES) measurements of in-plane band dispersions of  $4H_b$ - $\text{TaS}_{1.3}\text{Se}_{0.7}$ . (a) Intensity plot along  $\Gamma M$ . The right panel shows the zoomed area of the dashed box in the left graph. The two blue triangles indicate the folded  $\sqrt{13} \times \sqrt{13}$  Brillouin zone (BZ) boundary along  $\Gamma M$ , and the white dashed line represents the band bending position. (b) Crystal structure of  $4H_b$ - $\text{TaS}_{1.3}\text{Se}_{0.7}$ . (c) and (d) Top views of  $1T$  and  $1H$  layers, respectively. (e) and (f) Intensity plot along  $\Gamma K$  and  $MK$ , respectively. (g) and (h) Energy distribution curves (EDCs) of the dashed box area in (a) and (e), respectively. The blue EDC lines are at the folded BZ boundary. The peak positions of  $\alpha$  and  $\beta$  are marked with dashed lines. The inset of (g) shows the fitting of a typical EDC, with the shaded blue as the quasiparticle peak. The data are taken at  $T = 15$  K.

In this paper, ARPES measurements are performed on  $4H_b$ - $\text{TaS}_{1.3}\text{Se}_{0.7}$  to demonstrate the presence of an ultra-flat band below  $E_F$  in the CDW state. This flat band has an extremely narrow bandwidth and a sharp quasiparticle peak and extends over a large momentum range. By analyzing the orbital characters and layer-resolved band structures from the density functional theory (DFT) calculations, we confirm that the flat band results from the  $\sqrt{13} \times \sqrt{13}$  reconstruction in the top-most  $T$  layer. STM observes sharp peaks below and above  $E_F$  which are possibly caused by electron-correlation driven band splitting. The ultra-flat band with a nonzero filling factor sets the stage for studying the interaction of the correlated systems with extremely heavy electrons, such as superconductivity, Mott physics, spin-liquid state, heavy Fermion phenomenon, and magnetism.

## II. EXPERIMENT AND CALCULATION DETAILS

High-resolution ARPES measurements were performed at Renmin University with a Kr discharge lamp ( $h\nu = 10.05$  eV), the 03U and 09U Beamline of the SSRF (Shanghai, China), and the 13U Beamline in NSRL (Hefei, China) using photon energy between 20 and 90 eV. The samples were cleaved *in situ* with a vacuum better than  $6.5 \times 10^{-11}$  Torr at base temperature. The ARPES measurements were taken at a temperature of  $T = 15$  K, with an energy resolution of 5 meV unless otherwise stated. The STM experiments at  $T = 9$  K were conducted with an ultrahigh vacuum. Electrochemically

etched Pt-Ir tips calibrated on clean Ag(111) surfaces were used for all our STM measurements. The structure characterization of  $4H_b$ - $\text{TaS}_{1.3}\text{Se}_{0.7}$  was done by refined x-ray diffraction at room temperature [25].

The DFT calculations were performed with the QUANTUM ESPRESSO package [26]. The interactions between electrons and nuclei were described by the RRKJ-type ultrasoft pseudopotentials [27]. The atomic substitution in  $4H_b$ - $\text{TaS}_{1.3}\text{Se}_{0.7}$  was simulated with the virtual crystal approximation [28]. The generalized gradient approximation of the Perdew-Burke-Ernzerhof formula [29] was adopted for the exchange-correlation functional. The DFT-D3 method [30] was used to account for the van der Waals interaction. The band structure of the  $\sqrt{13} \times \sqrt{13}$  supercell was unfolded to that of the primitive cell by using the WANNIERTOOLS package [31]. The lattice constants of the CDW phase are  $a = b = 12.055$  Å,  $c = 24.002$  Å for unsubstituted and  $a = b = 12.222$  Å,  $c = 24.670$  Å with 0.7 Se substitution per formula, respectively.

## III. RESULTS AND DISCUSSION

The  $4H_b$ - $\text{Ta}(\text{S},\text{Se})_2$  is composed of interleaving  $T$ - $H$ - $T$ - $H$  layers with weak van der Waals interactions, where the crystal structure of  $T$  and  $H$  layers are octahedral and trigonal prismatic, respectively [Figs. 1(b)–1(d)]. The space group belongs to  $P6_3/mmc$ , and the crystal has an inversion symmetry with its inversion center located at the Ta of the  $T$  layer. In the

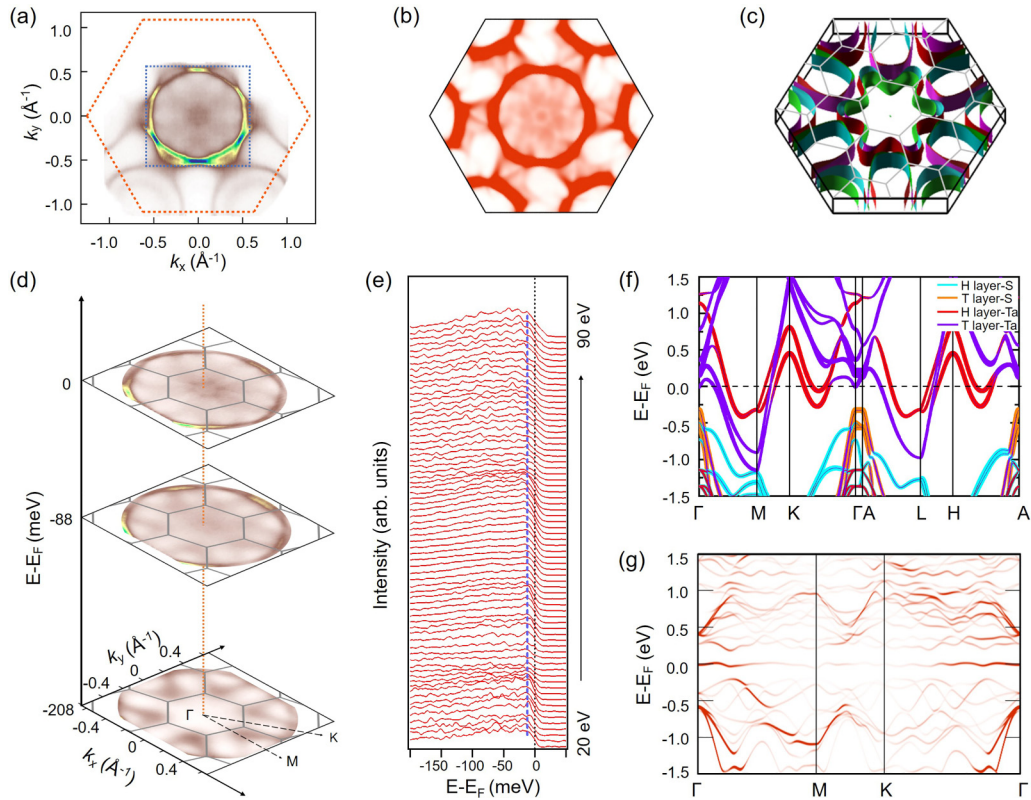


FIG. 2. Electronic structure of  $4H_b$ -TaS<sub>1.3</sub>Se<sub>0.7</sub>. (a) Fermi surface (FS) mapping using 50 eV photon energy. The orange line outlines the primary two-dimensional (2D) Brillouin zone (BZ). (b) Unfolded FS of the charge-density-wave (CDW) state from a slab calculation. (c) Calculated FS in the undistorted cell of the normal state. The black and gray lines represent the primary BZ and the folded BZ of the  $\sqrt{13} \times \sqrt{13}$  supercell, respectively. (d) Constant energy photoemission intensity maps at  $E_F$ ,  $E_F-88$  meV, and  $E_F-208$  meV, respectively. The coverage in momentum space is marked with the dashed square in (a). (e) Energy distribution curve (EDC) plots at the 2D BZ center with photon energies ranging from 20 to 90 eV, with an energy resolution of 15 meV. The blue dashed line marks the peak position of the flat band. (f) Layer- and element-resolved band structure of bulk  $4H_b$ -TaS<sub>1.3</sub>Se<sub>0.7</sub> in the normal state. (g) Unfolded band structure of freestanding  $1T$ -TaS<sub>1.3</sub>Se<sub>0.7</sub> monolayer by density functional theory (DFT) calculation. The data are taken at  $T = 15$  K.

pristine  $4H_b$ -TaS<sub>2</sub>, the most dominant CDW modulation is the  $\sqrt{13} \times \sqrt{13}$  distortion in the  $T$  layer, while the  $3 \times 3$  distortion in the  $H$  layer is strongly suppressed down to 15 K [32–34]. With the Se substitution of S, the CDW transition in the  $H$  layer is fully suppressed, and the system has  $T_{CDW} \sim 315$  K and an optimal superconducting transition temperature of  $T_c \sim 4.1$  K on  $4H_b$ -TaS<sub>1.3</sub>Se<sub>0.7</sub> [25].

The in-plane ARPES spectra of  $4H_b$ -TaS<sub>1.3</sub>Se<sub>0.7</sub> are shown in Fig. 1. From the figure, there exists a flat band ( $\alpha$ ) below  $E_F$  along the  $\Gamma M$  direction [Fig. 1(a)], which can be distinguished more clearly in the energy distribution curve (EDC) plot [Fig. 1(g)]. It locates  $\sim 15$  meV below  $E_F$ , with a small variation of  $\sim 9$  meV obtained by tracking the EDC peak positions. The peak width (half-width-half-maximum) is  $\sim 7$  meV [inset of Fig. 1(g)], which is limited by the experimental resolution. Considering the peak position, the narrow bandwidth, the finite peak width, and the low sample temperature, the possibility of a broad peak modulated by the Fermi cutoff can be excluded. The flat band feature is also clearly observed along another high-symmetry line  $\Gamma K$ , at the same energy and momentum range [Figs. 1(e) and 1(h)].

The flat band has been proposed in the CDW state of both bulk and monolayer  $1T$ -TaS<sub>2</sub> [16]. To confirm the connection between the flat band and the CDW state in the  $T$  layer, we

compare the measured electronic structure with the theoretical calculations. The ARPES intensity map at  $E_F$  in the CDW state is shown in Fig. 2(a). In the figure, the Fermi surface (FS) textures are characterized by a big hexagon-shaped pocket centered at the  $\Gamma$  point, dog-bone-shaped pockets around the  $M$  points, and round pockets around the  $K$  points [Fig. 2(a)]. In addition to these features, we observed more electronic states at the BZ center, inside the blue dashed square in Fig. 2(a). These intensities agree well with the unfolded FS in the CDW state from a slab calculation [Fig. 2(b)]. These states are absent in the normal state band calculations [Figs. 2(c) and 2(f)].

The DFT calculations on  $4H_b$ -TaS<sub>1.3</sub>Se<sub>0.7</sub> in both the normal and CDW states are performed. The normal state three-dimensional (3D) FSs and the layer- and element-resolved electronic band structures of the bulk  $4H_b$ -TaS<sub>1.3</sub>Se<sub>0.7</sub> are shown in Figs. 2(c) and 2(f), respectively. We can see that the electron states on the FS in the normal state are mainly contributed from the  $5d$  orbitals of Ta atoms. The big hexapetalous hole pockets around the  $\Gamma$  point are composed of two bands derived from the Ta atoms in  $T$  layer, shown as purple lines along  $\Gamma M$  in Fig. 2(f).

It is worth noting that the hexapetalous pockets are close to the  $\sqrt{13} \times \sqrt{13}$  reconstructed BZ boundary of the SD

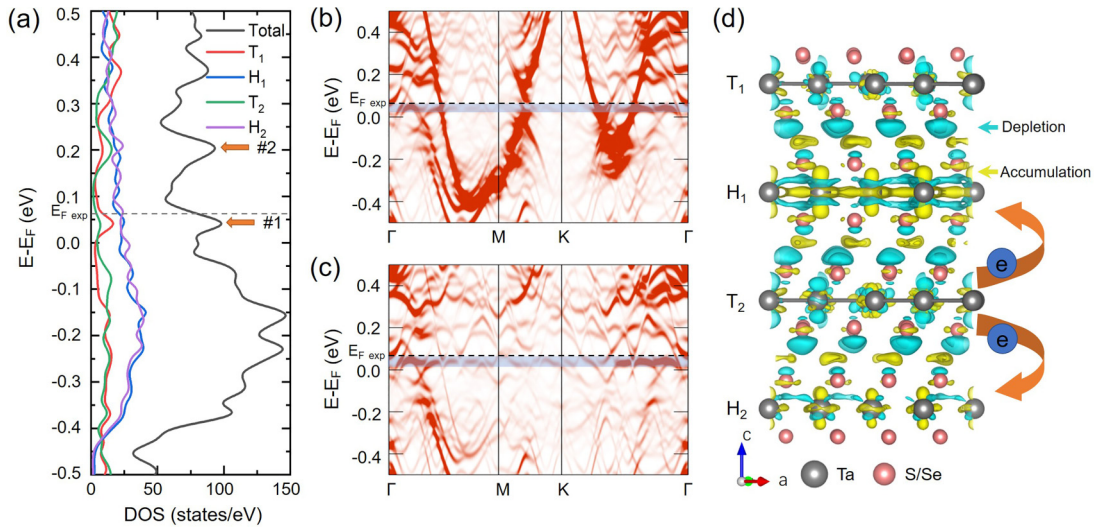


FIG. 3. Electronic properties of a  $T$ - $H$ - $T$ - $H$   $4H_b$ - $\text{TaS}_{1.3}\text{Se}_{0.7}$  slab in the charge-density-wave (CDW) state. (a) Total and layer-resolved density of states (DOS), smoothed with a Gaussian function. (b) Unfolded band structure of the 4L  $4H_b$ - $\text{TaS}_{1.3}\text{Se}_{0.7}$  slab. (c) Unfolded band structure with the orbital weights from the topmost  $T_1$  layer. (d) Three-dimensional charge difference densities of the 4L slab. Cyan and yellow isosurfaces represent the electron depletion and accumulation regions. The layers in the slab are labeled  $T_1$ ,  $H_1$ ,  $T_2$ , and  $H_2$ , respectively. The  $E_F^{\text{exp}}$  is the experimental Fermi level of angle-resolved photoemission spectroscopy (ARPES) results.

supercell. These two bands would be easily affected by the formation of SD and open gaps near  $E_F$  in the CDW state, resulting in the disappearance of the corresponding normal state FSs. As shown in the intensity plot data [Fig. 1(a)], the bending back energies of the bands are located at  $E_B = 88$  and 208 meV, respectively. Accordingly, we show the constant energy intensity plots at these two energies in Fig. 2(d) and find out that the bending back positions of these two bands are located at the folded BZ boundary. Along another high-symmetry direction ( $\Gamma K$  and  $MK$ ), the band bendings are also located at the reconstructed BZ boundaries in the CDW state [Figs. 1(e) and 1(f)]. Therefore, these band bendings are intimately related to the  $\sqrt{13} \times \sqrt{13}$  reconstruction.

After the CDW transition, new electron states emerge in the central region, mostly inside the first reconstructed BZ, at a low energy scale. It is more related to the formation of the  $\sqrt{13} \times \sqrt{13}$  supercell in the  $T$  layer. Meanwhile, the dog-bone-shaped FSs around  $M$  and the circular FSs around  $K$  [Fig. 2(a)], which are both derived from the Ta atoms in the  $H$  layer, remain intact after the CDW transition, which suggests that the electron states in the  $H$  layer are less affected by the formation of the CDW.

One noticeable difference between bulk  $1T$  and  $4H_b$  structures is their dimensionality. The  $1T$ - $\text{TaS}_2$  exhibits a few stacking orders and a dimerization along the  $c$  axis at low temperature in the CDW state. This dimerization has a strong  $k_z$  dispersion and introduces in-plane dispersion to the band [23,35,36]. In the  $4H_b$  system, the intercalation of the  $H$  layer reduces the 3D characteristics, as verified by the similar calculated band structures between  $\Gamma$ - $M$ - $K$  and  $A$ - $H$ - $L$  planes and the FSs [Figs. 2(c) and 2(f)], and turn the system more two-dimensional (2D) like. We did photon energy-dependent measurements in a wide range ( $h\nu = 20$ – $90$  eV) and confirmed the nearly 2D character of the flat band [Fig. 2(e)]. Comparing the experimental data shown in Fig. 1 and the band calculations, we find that the observed flat bands are substan-

tially different from the bulk  $1T$  TMDCs but more consistent with the band structure of a freestanding  $1T$ - $\text{TaS}_{1.3}\text{Se}_{0.7}$  monolayer [Fig. 2(g)].

Now we examine the momentum distribution of the flat band. In Figs. 1(a) and 1(e), the flat band  $\alpha$  extends over large momentum ranges along high-symmetry lines ( $\Gamma M$  and  $\Gamma K$ ) with the intensities decreasing rapidly beyond the first reconstructed BZ. The decay of the intensity at large momentum is attributed to Fourier components of the localized unpaired electron. When the unpaired electron localizes at the center of the SD, in momentum space, it also localizes within a finite range. According to Luttinger's theorem, the electron state over the whole BZ suggests integer numbers of electrons in a unit cell. With a nonzero filling factor of such a flat band below  $E_F$ , the electron correlation can be dominant, and a Mott insulating gap would appear.

To further confirm the origin of this flat band, we perform the calculations on a  $T$ - $H$ - $T$ - $H$  quadruple-layer (4L) slab of  $4H_b$ - $\text{TaS}_{1.3}\text{Se}_{0.7}$  in the CDW state and show the layer-projected electronic structures and density of states (DOS) in Fig. 3. The total DOS is shown in Fig. 3(a), which shows a peak (labeled as #1) with high DOS near  $E_F$ . According to the unfolded band structure shown in Figs. 3(b) and 3(c), the peak #1 corresponds to the flat band in the top-most  $T_1$  layer, as highlighted by the shaded region. The intensities are higher within  $\sim \frac{1}{3}$  of the BZ, as seen along the high-symmetry paths ( $\Gamma M$  and  $\Gamma K$ ), also in good accordance with our ARPES observations shown in Fig. 1. The layer-projected DOSs and band structures also show another flat band #2 located at  $\sim 150$ – $200$  meV above peak #1. This peak is from the  $T_2$  layer and is indirectly seen in the STM taken on the exposure of  $H$  layer, as marked in Fig. 4(c).

The charge transfer from the  $T$  layer to the  $H$  layer is illustrated by the 3D charge difference densities of a 4L slab calculation [Fig. 3(d)]. The electron depletion occurs in the  $T_1$  and  $T_2$  layers (cyan color), and the electron accumulation

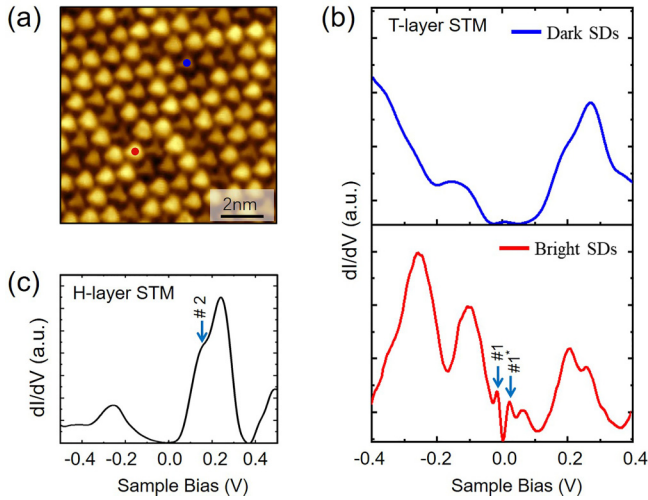


FIG. 4. Scanning tunneling spectroscopy (STM) spectra of  $4H_b$ - $\text{TaS}_{1.3}\text{Se}_{0.7}$  in the charge-density-wave (CDW) state. (a) Negative-bias-voltage STM topography taken on the  $1T_4H_b$  ( $V_S = -0.5$  V,  $I = -60$  pA). Red and blue dots are indications of bright and dark Stars of David (SDs), respectively. (b) Typical conductivity ( $dI/dV$ ) spectra taken on a bright SD (lower panel) and dark SD (upper panel) of (a). (c) A typical  $dI/dV$  spectrum acquired at  $1H_4H_b$ .

appears in the  $H_1$  and  $H_2$  layers (yellow color). In comparison with the bulk  $1T$  structure, the charge transfer from the  $T$  layer to the  $H$  layer in the  $4H_b$  system shifts the  $T$ -layer-related bands up. Meanwhile, as seen from the figure, the top-most  $T_1$  layer loses fewer electrons than the bulklike  $T_2$  layer due to the missing of a  $H$  layer on its top. Thus, we assign the flat band  $\alpha$  to peak #1 from the top-most  $T_1$  layer by comparing the ARPES data with the 4L slab results from DFT calculations.

The STM topography measurement at the CDW state is shown in Fig. 4(a). In the  $T$  layer of  $4H_b$ - $\text{TaS}_2$ , 12 Ta  $5d$  electrons pair to form six occupied bands within one SD, leaving one unpaired localized electron in a half-filled band. In  $4H_b$ - $\text{TaS}_{1.3}\text{Se}_{0.7}$ , the Se doping, with different atom sizes and electron-negativity from S, effectively decreases the number of localized electrons, resulting in partially filled SDs [19]. The bright/dark spots in the figure are the SDs with/without the unpaired electron. We take typical STM spectra on both bright and dark SDs and show them in Fig. 4(b). From the spectrum of the bright SD, a DOS peak is located at 15 meV below  $E_F$  (labeled as #1), showing consistency among ARPES, STM, and DFT results. These suggest that the peak #1 is intimately related to the flat band  $\alpha$ . In addition, an extra peak of  $\sim 30$  meV above  $E_F$  labeled as #1\* is observed. These two peaks give a small gap ( $\Delta \sim 45$  meV). In contrast, from the spectrum of the dark SD, no sharp peak feature is observed near  $E_F$ . We note that the peaks #1 and #1\* always appear/disappear in pairs. This double-peak feature was not reported on  $4H_b$ - $\text{TaS}_2$ , but only one peak above  $E_F$  was observed [33,37]. With the substitution of Se for S, the bands near  $E_F$  slightly shift down, and correspondingly, the  $\alpha$  flat band moves from above to below  $E_F$ , where the electron correlation becomes nonnegligible. For a flat band with an

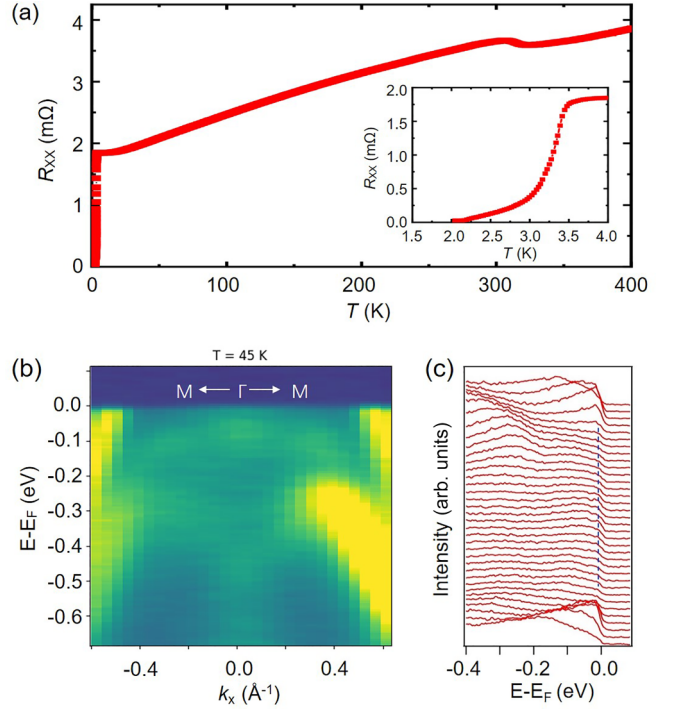


FIG. 5. (a) Temperature dependence of in-plane resistivity ( $R_{xx}$ ) of  $4H_b$ - $\text{TaS}_{1.3}\text{Se}_{0.7}$ . Inset: Zoom in at low temperature. (b) Intensity plot of  $4H_b$ - $\text{TaS}_{1.3}\text{Se}_{0.7}$  at  $T = 45$  K along  $\Gamma$ - $M$ . (c) Energy distribution curve (EDC) plot of (a). The dashed line indicates the flat band near  $E_F$ .

extremely small bandwidth, a considerably small Hubbard interaction  $U$  would be sufficient to cause a band splitting [38]. Comparing with the gap in  $1T$ - $\text{TaS}_2$ , the small gap size of  $\sim 45$  meV could be due to the modification of the bandwidth [39] and/or the screening of the Coulomb interaction by the insertion of a conducting  $H$  layer.

Another consideration of the origin of the peak is the Kondo effect, where itinerant electrons are scattered by magnetic impurities. STM measurement showed a sharp peak slightly above  $E_F$  in pristine  $4H_b$ - $\text{TaS}_2$ , and it was attributed to the Kondo effect [40]. In this  $4H_b$ - $\text{TaS}_{1.3}\text{Se}_{0.7}$ , this flat band should have a different origin. First, as shown in Fig. 5(a), the transport measurement shows no sign of the Kondo effect in  $4H_b$ - $\text{TaS}_{1.3}\text{Se}_{0.7}$ , consistent with previous reports [25]. Second, we take the ARPES intensity map along  $\Gamma$ - $M$  and the corresponding EDC plot at  $T = 45$  K, which is far above the Kondo temperature reported in pristine  $4H_b$ - $\text{TaS}_2$ , and show it in Figs. 5(b) and 5(c). In the figure, the flat band still exists at the elevated temperature, which rules out the possibility of the Kondo effect in this  $T$ - $H$ - $T$ - $H$  heterostructure. The last is that the STM spectra show the appearance/disappearance of the peaks below and above  $E_F$  in pairs, as shown in Fig. 4. Hereby, the well-defined flat band in  $4H_b$ - $\text{TaS}_{1.3}\text{Se}_{0.7}$  is unlikely from the Kondo effect.

In addition to the flat bands, there exist more features near the BZ center. One is a narrow band, labeled as  $\beta$ , located  $\sim 75$  meV below  $E_F$  with a wider bandwidth of up to 50 meV and weaker intensity. According to the freestanding  $1T$ - $\text{Ta}(\text{S}, \text{Se})_2$  monolayer calculation [Fig. 2(g)], we can see that the  $\beta$

feature is absent. Therefore, this band is most likely related to the hybridization between the  $T$  and  $H$  layers in the  $4H_b$  structure, which deserves more detailed study in the future. Another is an electronlike band with a fast dispersion which is from Ta  $5d$  orbital crosses with the flat band and gives the intensity variation in the FS mapping shown in Fig. 2(a). The hybridization between a fast dispersion and a flat band provides a platform to study the Kondo interaction normally found in  $f$ -electron systems.

#### IV. CONCLUSIONS

Our ARPES observation of the almost dispersionless band presented unambiguous evidence of a flat band with an extremely narrow bandwidth of 9 meV below  $E_F$ . By using STM, we identified the narrow bands showing a sharp peak in local DOS, belonging to a pair of peaks below and above the Fermi level at the center of a SD. This leaves a gap size of 45 meV, which we attribute to the localization of Mott electrons. In condensed matter, with the dominance of electron interaction and controlling of the filling of the band, many physics phenomena such as Mott insulators, ferromagnetism, and high- $T_c$  superconductivity have been reported [41–51]. With a narrow bandwidth, a considerably small Coulomb interaction or electron correlation could be effective enough to drive many correlation-related quantum phenomena, such as the superconductivity in twisted bilayer graphene [10,11].

The TMD with  $4H_b$  structure provides an ideal platform with a smaller energy scale to finetuning of the flat band to achieve such exotic phenomena [52,53].

#### ACKNOWLEDGMENTS

This paper was supported by the National Natural Science Foundation of China (Grants No. 12274455, No. 12174443, No. 12222413, No. 11674326, and No. 11874357), the National Key R&D Program of China (Grants No. 2022YFA1403800, No. 2017YFA0302903, No. 2018YFE0202600, No. 2022YFA1403203, No. 2022YFB3608000, and No. 2021YFA1600201), the Beijing Natural Science Foundation (Grant No. Z200005), the Joint Funds of the National Natural Science Foundation of China and the Chinese Academy of Sciences' Large-Scale Scientific Facility (Grants No. U1832141, No. U1932217, No. U2032215, and No. U2032215), the Natural Science Foundation of Shanghai (Grants No. 22ZR1473300 and No. 23ZR1482200), the Fundamental Research Funds for the Central Universities, and the Research Funds of Renmin University of China (Grants No. 18XNLG14, No. 21XNLG27, and No. 19XNLG17). Computational resources were provided by the Physical Laboratory of High-Performance Computing at Renmin University of China. We would also like to show our gratitude to Kun Jiang for his comments on our manuscript and fruitful discussion.

- 
- [1] W.-X. Qiu, S. Li, J.-H. Gao, Y. Zhou, and F.-C. Zhang, *Phys. Rev. B* **94**, 241409(R) (2016).
- [2] M. R. Slot, T. S. Gardenier, P. H. Jacobse, G. C. Van Miert, S. N. Kempkes, S. J. Zevenhuizen, C. M. Smith, D. Vanmaekelbergh, and I. Swart, *Nat. Phys.* **13**, 672 (2017).
- [3] R. Drost, T. Ojanen, A. Harju, and P. Liljeroth, *Nat. Phys.* **13**, 668 (2017).
- [4] H. Ozawa, S. Taie, T. Ichinose, and Y. Takahashi, *Phys. Rev. Lett.* **118**, 175301 (2017).
- [5] F. Baboux, L. Ge, T. Jacqmin, M. Biondi, E. Galopin, A. Lemaître, L. Le Gratiet, I. Sagnes, S. Schmidt, H. E. Türeci, A. Amo, and J. Bloch, *Phys. Rev. Lett.* **116**, 066402 (2016).
- [6] T. Jacqmin, I. Carusotto, I. Sagnes, M. Abbarchi, D. D. Solnyshkov, G. Malpuech, E. Galopin, A. Lemaître, J. Bloch, and A. Amo, *Phys. Rev. Lett.* **112**, 116402 (2014).
- [7] B. Corcoran, C. Monat, C. Grillet, D. J. Moss, B. J. Eggleton, T. P. White, L. O'Faolain, and T. F. Krauss, *Nat. Photon.* **3**, 206 (2009).
- [8] I. Hase, T. Yanagisawa, and K. Kawashima, *Nanomaterials* **9**, 876 (2019).
- [9] M. Han, H. Inoue, S. Fang, C. John, L. Ye, M. K. Chan, D. Graf, T. Suzuki, M. P. Ghimire, W. J. Cho *et al.*, *Nat. Commun.* **12**, 5345 (2021).
- [10] Y. Cao, V. Fatemi, S. Fang, K. Watanabe, T. Taniguchi, E. Kaxiras, and P. Jarillo-Herrero, *Nature (London)* **556**, 43 (2018).
- [11] Y. Cao, V. Fatemi, A. Demir, S. Fang, S. L. Tomarken, J. Y. Luo, J. D. Sanchez-Yamagishi, K. Watanabe, T. Taniguchi, E. Kaxiras *et al.*, *Nature (London)* **556**, 80 (2018).
- [12] D. Pei, B. Wang, Z. Zhou, Z. He, L. An, S. He, C. Chen, Y. Li, L. Wei, A. Liang *et al.*, *Phys. Rev. X* **12**, 021065 (2022).
- [13] L. Wang, E.-M. Shih, A. Ghiotto, L. Xian, D. A. Rhodes, C. Tan, M. Claassen, D. M. Kennes, Y. Bai, B. Kim *et al.*, *Nat. Mater.* **19**, 861 (2020).
- [14] Z.-Y. Liu, S. Qiao, B. Huang, Q.-Y. Tang, Z.-H. Ling, W.-H. Zhang, H.-N. Xia, X. Liao, H. Shi, W.-H. Mao *et al.*, *Nano Lett.* **21**, 7005 (2021).
- [15] W. Ruan, Y. Chen, S. Tang, J. Hwang, H.-Z. Tsai, R. L. Lee, M. Wu, H. Ryu, S. Kahn, F. Liou *et al.*, *Nat. Phys.* **17**, 1154 (2021).
- [16] P. Darancet, A. J. Millis, and C. A. Marianetti, *Phys. Rev. B* **90**, 045134 (2014).
- [17] L. Cheng, X. Long, X. Chen, X. Zou, and Z. Liu, *Phys. Rev. B* **104**, L241114 (2021).
- [18] D. Pasquier and O. V. Yazyev, *Phys. Rev. B* **98**, 045114 (2018).
- [19] S. Qiao, X. Li, N. Wang, W. Ruan, C. Ye, P. Cai, Z. Hao, H. Yao, X. Chen, J. Wu *et al.*, *Phys. Rev. X* **7**, 041054 (2017).
- [20] J. A. Wilson, F. Di Salvo, and S. Mahajan, *Adv. Phys.* **24**, 117 (1975).
- [21] K. Rossnagel and N.V. Smith, *Phys. Rev. B* **73**, 073106 (2006).
- [22] J.-J. Kim, W. Yamaguchi, T. Hasegawa, and K. Kitazawa, *Phys. Rev. Lett.* **73**, 2103 (1994).
- [23] Y. D. Wang, W. L. Yao, Z. M. Xin, T. T. Han, Z. G. Wang, L. Chen, C. Cai, Y. Li, and Y. Zhang, *Nat. Commun.* **11**, 4215 (2020).
- [24] H. Lin, W. Huang, K. Zhao, S. Qiao, Z. Liu, J. Wu, X. Chen, and S.-H. Ji, *Nano Res.* **13**, 133 (2020).
- [25] Y. Liu, L. Li, W. Lu, R. Ang, X. Liu, and Y. Sun, *J. Appl. Phys.* **115**, 043915 (2014).

- [26] P. Giannozzi, S. Baroni, N. Bonini, M. Calandra, R. Car, C. Cavazzoni, D. Ceresoli, G. L. Chiarotti, M. Cococcioni, I. Dabo *et al.*, *J. Phys.: Condens. Matter* **21**, 395502 (2009).
- [27] A. M. Rappe, K. M. Rabe, E. Kaxiras, and J. D. Joannopoulos, *Phys. Rev. B* **41**, 1227 (1990).
- [28] Y. Ge, F. Zhang, and Y. Yao, *Phys. Rev. B* **93**, 224513 (2016).
- [29] J. P. Perdew, K. Burke, and M. Ernzerhof, *Phys. Rev. Lett.* **77**, 3865 (1996).
- [30] S. Grimme, J. Antony, S. Ehrlich, and H. Krieg, *J. Chem. Phys.* **132**, 154104 (2010).
- [31] Q. Wu, S. Zhang, H.-F. Song, M. Troyer, and A. A. Soluyanov, *Comput. Phys. Commun.* **224**, 405 (2018).
- [32] J. Narayan, *Appl. Phys. Lett.* **29**, 223 (1976).
- [33] C. Wen, J. Gao, Y. Xie, Q. Zhang, P. Kong, J. Wang, Y. Jiang, X. Luo, J. Li, W. Lu *et al.*, *Phys. Rev. Lett.* **126**, 256402 (2021).
- [34] A. Ribak, R. M. Skiff, M. Mograbi, P. Rout, M. Fischer, J. Ruhman, K. Chashka, Y. Dagan, and A. Kanigel, *Sci. Adv.* **6**, eaax9480 (2020).
- [35] T. Ritschel, H. Berger, and J. Geck, *Phys. Rev. B* **98**, 195134 (2018).
- [36] S.-H. Lee, J. S. Goh, and D. Cho, *Phys. Rev. Lett.* **122**, 106404 (2019).
- [37] V. Vaño, M. Amini, S. C. Ganguli, G. Chen, J. L. Lado, S. Kezilebieke, and P. Liljeroth, *Nature (London)* **599**, 582 (2021).
- [38] Y. Nakata, K. Sugawara, A. Chainani, H. Oka, C. Bao, S. Zhou, P.-Y. Chuang, C.-M. Cheng, T. Kawakami, Y. Saruta *et al.*, *Nat. Commun.* **12**, 5873 (2021).
- [39] C. J. Butler, M. Yoshida, T. Hanaguri, and Y. Iwasa, *Nat. Commun.* **11**, 2477 (2020).
- [40] S. Shen, T. Qin, J. Gao, C. Wen, J. Wang, W. Wang, J. Li, X. Luo, W. Lu, Y. Sun *et al.*, *Chin. Phys. Lett.* **39**, 077401 (2022).
- [41] S. Miyahara, S. Kusuta, and N. Furukawa, *Physica C: Superconductivity* **460-462**, 1145 (2007).
- [42] H. Aoki, *J. Supercond. Novel Magn.* **33**, 2341 (2020).
- [43] A. Kononov, M. Endres, G. Abulizi, K. Qu, J. Yan, D. G. Mandrus, K. Watanabe, T. Taniguchi, and C. Schönenberger, *J. Appl. Phys.* **129**, 113903 (2021).
- [44] G. E. Volovik, *JETP Lett.* **107**, 516 (2018).
- [45] D. Yudin, D. Hirschmeier, H. Hafermann, O. Eriksson, A. I. Lichtenstein, and M. I. Katsnelson, *Phys. Rev. Lett.* **112**, 070403 (2014).
- [46] G. Volovik, *Pis'ma Zh. Eksp. Teor. Fiz.* **59**, 798 (1994) [*JETP Lett.* **59**, 830 (1994)].
- [47] I. Hase, T. Yanagisawa, Y. Aiura, and K. Kawashima, *Phys. Rev. Lett.* **120**, 196401 (2018).
- [48] A. Mielke and H. Tasaki, *Commun. Math. Phys.* **158**, 341 (1993).
- [49] A. Mielke, *J. Phys. A: Math. Gen.* **32**, 8411 (1999).
- [50] H. Tasaki, *Prog. Theor. Phys.* **99**, 489 (1998).
- [51] J.-Y. You, B. Gu, and G. Su, *Sci. Rep.* **9**, 20116 (2019).
- [52] D. Lee, K.-H. Jin, F. Liu, and H. W. Yeom, *Nano Lett.* **22**, 7902 (2022).
- [53] L. Tarruell, D. Greif, T. Uehlinger, G. Jotzu, and T. Esslinger, *Nature (London)* **483**, 302 (2012).